PAPER

Check for updates

Encapsulated liquid nano-droplets for efficient and selective biphasic hydroformylation of long-chain alkenes†

Xiaoli Zhang,[a] Juan Wei [ID] *[b] and Xiaoming Zhang*[c]

Aqueous nano-droplets of homogeneous Rh-TPPTS catalyst encapsulated within the cavity of hollow silica nanospheres were fabricated for biphasic hydroformylation of long-chain alkenes, which showed significant reaction rate enhancement effects and improved aldehyde selectivity.

As a typical water medium biphasic catalysis system, the Ruhrchemie/Rhone-Poulenc (RCH/RP) process with water-soluble Rh-tris(*m*-sulfonatophenyl)phosphine (Rh-TPPTS) complexes as catalysts has been successfully employed for the industrial hydroformylation of C3–C4 olefins.[1–3] The superior advantages like sustainable water as a solvent, easy separation and recycling make this method meaningful and fascinating. However, the reaction occurs at a sufficient rate only for lighter alkenes that have relatively high solubility in water where the reaction takes place. Severe mass transport resistance is encountered for long-chain olefins with poor water solubility, since the reaction can only take place slowly at the water/ organic interface. To solve the mass transport problems, many strategies have been developed, such as addition of organic co-solvents, amphiphilic surfactants, cyclodextrins, and polymer lattices or anchoring the metal catalyst to the hydrophobic part of surfactants that self-organize in micellar form.[4–8] Although these attempts indeed are able to improve the catalytic efficiency, the extra additives or amphiphilic ligands often cause difficulty in separating and purifying the final products.

Emulsions, which are composed of micro-droplet or nano-droplet suspensions in an immiscible fluid, have attracted much research attention for biphasic catalysis.[9–14] The large organic–aqueous interfacial areas significantly facilitate the diffusion-limited phase transfer of molecules across an interface, and can improve the interfacial reaction efficiency by orders of magnitude compared to macroscopic systems. Among various types of emulsions, solid colloidal particle stabilized micro-droplets are especially fascinating because of their stability and easier separation process.[15] Recently, Yang's group applied a solid particle stabilized Pickering emulsion system to the hydroformylation of long-chain olefins.[16] And due to the greatly increased interface area, the Pickering emulsion system exhibits much higher activity and aldehyde selectivity in hydroformylation of 1-octene compared to the neat water/oil biphasic system. Moreover, it has been demonstrated that the emulsion droplet size influences the oil–water interface significantly, and with smaller droplet sizes, larger interface area can be obtained, leading to enhanced catalytic activity.[16,17] Nevertheless, for solid colloidal particle stabilized emulsions, the droplet sizes could only be tuned to the micro-meter scale. It is really difficult and challenging to make nanometer sized emulsion droplets. On the other hand, supported liquid phase catalysts on solids have been proposed as another promising pathway to circumvent the problem of mass transport, due to their relatively short diffusion distance in a thin liquid layer.[18,19] However, the required thin liquid layer in traditional porous materials may limit their benefit as an ideal homogeneous microenvironment. Overcoming these limitations, hollow structured mesoporous nanospheres might have great potential owing to their superior properties, such as excellent loading capacity, good permeability and faster mass transport *etc.* However, seldom are reports seen on such investigations.[20–22]

Herein, in this study, we proposed a general encapsulation method for fabricating nanoscale droplets of aqueous phase homogeneous catalyst Rh-TPPTS suspended in organic surroundings for biphasic hydroformylation of long-chain alkenes. As shown in Fig. 1, the water-soluble rhodium catalyst dissolved in the aqueous phase was confined into the hollow cavity of monodisperse mesoporous silica nanoreactors, and due to the isolation effects of the outer shell, discrete nanodroplets could be formed. Due to the immiscible features of an aqueous

[a] Shaanxi Key Laboratory of Natural Products & Chemical Biology, College of Chemistry & Pharmacy, Northwest A&F University, 22 Xinong Road, Yangling 712100, Shaanxi, P. R. China

[b] School of Chemical and Environmental Engineering, Sichuan University of Science and Engineering, Zigong 643000, P. R. China. E-mail: jwei@suse.edu.cn

[c] School of Chemistry and Chemical Engineering, Shanxi University, Wucheng Road 92, Taiyuan 030006, P. R. China. E-mail: xmzhang4400@sxu.edu.cn

† Electronic supplementary information (ESI) available: Experimental details and additional information about material characterization. See DOI: 10.1039/c9nj02493j
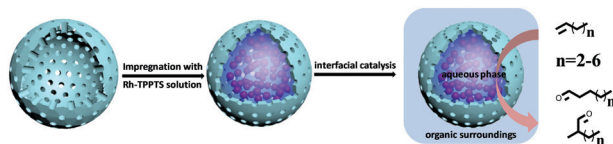
Fig. 1   Illustration of confined aqueous phase catalysis in hollow silica nanoreactors.

catalyst solution with its organic surroundings, the aqueous droplets could be well dispersed in an organic medium. The resulting large aqueous–organic surface contact area could thus improve the mass transfer rate and facilitate the reaction efficiency.

Hollow structured mesoporous silica nanoreactors (HMSN) were synthesized through a facile *in situ* generated template method in a one-pot medium by utilizing the etching effects of organosilane 1,2-bis(triethoxysilyl)ethane (BTEE, for the experiment procedures, see the ESI†).[23,24] As shown in Fig. S1 (ESI†), the scanning electron microscopy (SEM) image at low magnification shows that they are made up of uniform nanospheres with diameters of 100 ± 20 nm. Transmission electron microscopy (TEM) observation further reveals that hollow structured silica nanospheres with a uniform particle size of 80–120 nm and a shell thickness of 15 nm are successfully produced (Fig. 2a). Ordered mesopores with diameters of about 2–3 nm throughout the shells could be clearly observed. The high-magnification image further shows that the mesochannels are continuous throughout the shell with openings at the surface and are radially oriented to the nanosphere surface, which means that the mesochannels of the hollow nanospheres are readily accessible (Fig. 2b). The nitrogen sorption isotherm and the corresponding pore size distribution curve of the HMSN sample are shown in Fig. 2c and d. A typical type-IV isotherm with a sharp capillary condensation step and a large H1 type

hysteresis loop in the relative pressure (P/P_0) range of 0.45–1.0 is observed, indicating characteristics of a mesoporous material with a narrow pore size distribution. The Barrett–Joyner–Halenda (BJH) pore size distribution confirms that the uniform mesopore size is centered around 2.4–2.6 nm, which is big enough for the diffusion of most organic molecules. The Brunauer–Emmett–Teller (BET) surface area and total pore volume of the HMSN are measured to be as high as 702 m^2 g^{-1} and 0.974 cm^3 g^{-1} respectively, which will be beneficial for the following introduction of the aqueous homogeneous catalyst solution and the catalytic process.

The Rh-TPPTS catalyst solution was inserted into the cavity of the HMSN through a simple impregnation method. Since the amount of water solvent might influence the freedom and concentration of the entrapped catalyst significantly, therefore, entrapped homogeneous catalysts with different amounts of water were produced. And the yielded solid catalysts are still in the powder state, denoted as Rh-TPPTS-χ@HMSN, where χ represents the volume of the catalyst solution used as described in the ESI.† The entrapped contents of the homogeneous catalyst solution were measured using the thermogravimetric analysis (TGA) technique (Fig. 3a). The weight loss below 200 °C corresponds to the loss of trapped water solvent and the weight loss between 200 and 800 °C is from the decomposition of the Rh-TPPTS catalyst within the HMSN. As can be seen, the water content increases from 20.9% to 63.9% as χ ranges from 0.27 to 1.37. The formation of a homogeneous catalyst micro-droplet within the HMSN was demonstrated by fluorescence confocal microscopy (CLMS) observations. A water soluble dye, fluorescein isothiocyanate (FITC), was selected as the probe molecule. As shown in Fig. 3b, the CLMS image of FITC@HMSN dispersions in toluene shows the presence of discrete objects, indicating that the aqueous solution could be confined within the HMSN cavity and no agglomerates of aqueous solution were formed.

To explore the catalytic potential of this catalyst, the hydroformylation of 1-octene as a model was firstly performed. This olefin has a sufficiently long chain to reduce its water solubility and to render biphasic situations. Hence, the hydroformylation of this substrate is a good model reaction to verify the efficiency of our new aqueous biphasic approach. The mini-size of our confined catalyst is expected to be adequate for the reaction without addition of co-solvents or surfactants. For comparison,
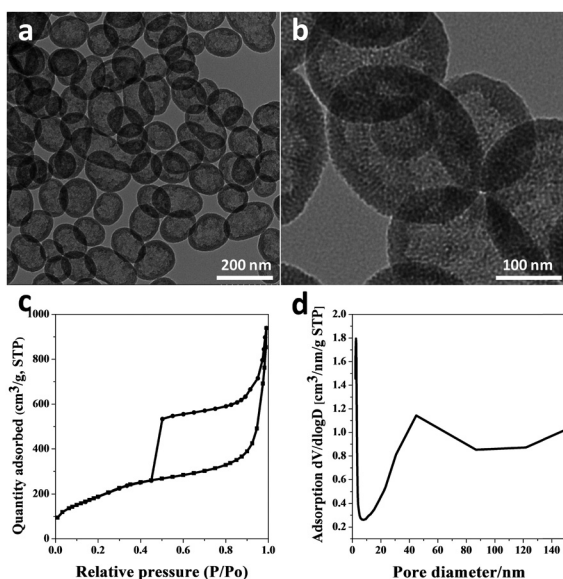

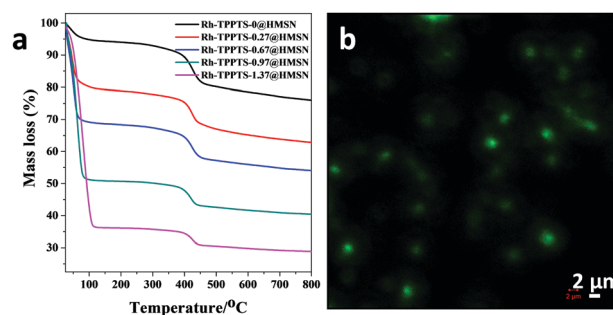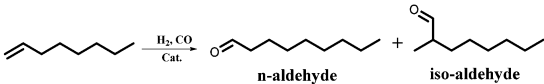
Fig. 2   (a and b) TEM images of HMSN with different magnifications, and (c and d) nitrogen sorption isotherm and the corresponding pore size distribution curve.

Fig. 3   (a) TGA of Rh-TPPTS-χ@HMSN samples, and (b) CLMS of FITC-0.97@HMSN.

Table 1 Comparisons of the catalytic performance of Rh-TPPTS in biphasic, micelle, Pickering emulsion, supported aqueous-phase catalysis (SAPC) and nano-confined aqueous catalysis systems, and the catalytic results under different reaction conditions[a]

Entry	Catalytic system	Conv.[b] (%)	Sel.[b] (%)	n/b[c]	TOF[d] (h^{-1})
1	Biphasic[e]	22.4	39.6	68/32	96
2	CTAB additive[f]	48.0	49.3	70/30	124
3	Rh-TPPTS-0.97@HMSN[g]	>99	76.0	69/31	623
4	Supported aqueous-phase	51.3	45.8	69/31	255
5	Pickering emulsion	61.9	51.8	69/31	348
6	Rh-TPPTS-0.97@HMSN[h]	75.6	68.5	69/31	—
7	Rh-TPPTS-0.97@HMSN[i]	96.8	77.5	68/32	—
8	Rh-TPPTS-0.97@HMSN[j]	86.8	70.8	68/32	—
9	Rh-TPPTS-0.97@HMSN[k]	93.5	76.5	69/31	—
10	Rh-TPPTS@HMSN (run2)	35.0	46.1	69/31	—
11	Rh-TPPTS@C_1-HMSN	>99	76.2	68/32	378
12	Rh-TPPTS@C1-HMSN (run4)	95.4	73.0	68/32	—
13	Rh-TPPTS@C_8-HMSN	>99	72.4	69/31	558
14	Rh-TPPTS@C_8-HMSN (run4)	76.4	70.5	69/31	—

[a] Reaction conditions: solid catalyst (Rh = 2.5 μmol, Rh/TPPTS ratio is 1/5), 7.5 mmol 1-octene, toluene as the solvent (containing dodecane as an internal standard), 70 °C, 30 bar of CO/H_2, 7 h. [b] Analysis by GC, aldehyde selectivity, the by-products are from alkene isomerization, alkene reduction and aldehyde reduction. [c] Normal/branched. [d] Calculated below 30% conversion. [e] Stirring rate is 750 rpm. [f] CTAB = 10 mg, reaction time is 9 h. [g] Reaction time is 5 h. [h] Reaction temperature is 60 °C. [i] Reaction temperature is 80 °C and reaction time is 3 h. [j] Reaction pressure is 20 bar. [k] Reaction pressure is 40 bar and reaction time is 4 h.

some aqueous biphasic approaches, including traditional biphasic systems, use of a surfactant as an additive, Pickering emulsion systems and supported aqueous-phase catalysts (SAPCs), have been extensively investigated. In order to directly compare these different strategies, similar operating conditions were used (343 K and 30 bar of CO/H_2 pressure). The catalytic results are summarized in Table 1.

The water–oil biphasic system only affords a 22.4% conversion with an aldehyde selectivity of 39.6% (entry 1). The by-products are mainly isomeric olefins, octane or alcohols generated from isomerization and hydrogenation of 1-octene or excessive hydrogenation of aldehyde products. The low activity and selectivity of the water–oil biphasic system should be ascribed to the severe diffusion barrier arising from the poor water solubility. For improving the catalytic performance, CTAB (hexadecyltrimethyl ammonium bromide) as a surfactant was firstly added to the biphasic system. And the reaction rate was indeed enhanced, while the aldehyde selectivity and n/b ratio also increased (entry 2), which is consistent with a literature report that the formation of CTAB micelles could provide an ordered and compact microenvironment to promote the efficiency.[25] Encouragingly, the confined catalyst Rh-TPPTS@HMSN system affords much higher activity and aldehyde selectivity than the CTAB micelle system under similar reaction conditions. The conversion could reach as high as >99% within 5 h, and the aldehyde selectivity increases to 76.2% with an n/b ratio of 69/31 (entry 3). The TOF of our confined catalysis system could be increased to 623 h^{-1}, much higher than 124 h^{-1} for the CTAB micelle system and 96 h^{-1} for the biphasic system. Obviously, much better catalytic performance was obtained by using the novel confined catalysis system. The enhanced activity might be related to the following factors. Firstly, the unique hollow structure of the HMSN with thin shell thickness, and large surface area and pore volume is beneficial for the exposure of active sites and mass transport of substrates. Secondly, due to the isolated effects of the outer shell, the confined aqueous droplets are limited to decades of nanometers and suspended in the organic phase, therefore, the oil–water interface areas are increased remarkably. Moreover, the catalysts can move as free as a homogeneous catalyst in the confined space, which has been reported to benefit the catalytic activity.[26–28] With the reaction rates being significantly reinforced, the reaction time for side reactions might be shortened, leading to higher chemoselectivity. However, the enhanced reaction rates and decreased side reactions would not influence the regioselectivity, which is mainly determined by the steric configuration of the metal–ligand–reactant complex, affording similar n/b values of the aldehyde products.

To clarify these factors, some comparable reactions were performed. For example, a supported aqueous-phase catalyst (SAPC), which was formed by subtly adsorbing a thin aqueous layer containing water-soluble catalyst Rh-TPPTS onto a hydrophilic mesoporous support SBA-15 (BET surface area 445 $m^2 g^{-1}$, pore volume 0.59 $cm^3 g^{-1}$, see Fig. S2 (ESI†); for the preparation procedures, see the Experimental section in the ESI†) was also used. Due to the increased interfacial area between the aqueous and the organic phase, the hydroformylation rate was efficiently increased, 51.3% conversion and 45.8% aldehyde selectivity could be obtained (entry 4). However, because of the long hydrophilic channel in bulk SBA-15, it is difficult for the organic reactants to diffuse through the pore to contact with the catalyst, yielding a limitation of such a method. This result also suggests the superior advantage of the HMSN support. Moreover, a micrometer-sized Pickering emulsion was also formed to increase the oil–water interfacial area (for the preparation procedures, see the Experimental section in the ESI†). As shown in Fig. S3 (ESI†), partially hydrophobic silica
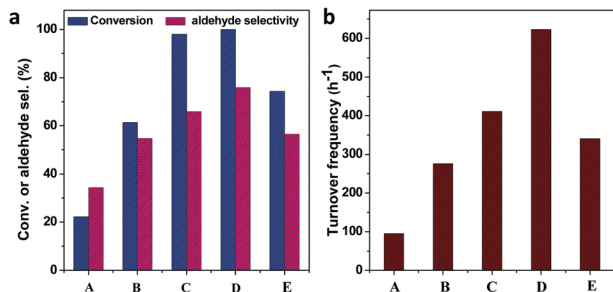
Fig. 4 Catalytic results of Rh-TPPTS-χ@HMSN with different amounts of water (1-octene as a substrate), (A) Rh-TPPTS-0@HMSN, (B) Rh-TPPTS-0.27@HMSN, (C) Rh-TPPTS-0.67@HMSN, (D) Rh-TPPTS-0.97@HMSN, and (E) Rh-TPPTS-1.37@HMSN.

nanospheres with a particle size of 40–60 nm were used as an emulsifier to stabilize the water-in-oil Pickering emulsions. The optical micrograph shows that the average size of the emulsion droplets was *ca.* 85 μm. The Pickering emulsion system affords higher activity (entry 5, 61.9% conversion, TOF 348 h^{-1}) and aldehyde selectivity (51.8%) than the CTAB additive system and supported aqueous phase system under similar reaction conditions. However, because of the micrometer scale, the interface area is much smaller than our confined aqueous catalysis system. Therefore, compared with Rh-TPPTS@HMSN, the reaction rate was much lower.

The influence of the water content confined in the HMSN towards the reaction efficiency was also investigated. As shown in Fig. 4, without water as a dissolving solvent, Rh-TPPTS-0@HMSN showed poor catalytic activity, only 22.2% conversion and 34.4% aldehyde selectivity were obtained, which might be attributed to the non-free state of catalyst molecules.[18,19,29] By increasing the water content from 20.9% to 63.9%, the activity of the confined solid catalyst increases first and reaches a maximum with a content of 49.3% (>99% conversion, TOF 623 h^{-1}). After that, the activity of the solid catalyst decreases by further increasing the water amount. The "volume active site density" of the nano-cavity and freedom degree of the confined catalyst can be used to explain this tendency.[30] With the increase in water content from 20.9% to 49.3%, the density of catalyst molecules in the water droplet decreases. Also, the freedom degree of the catalyst molecules was improved. Consequently, the exposure and contact frequency between the substrates and catalysts increased, and the activity of the solid catalyst also increased. At high water content, the outer surface was also surrounded by aqueous solution, which makes the diffusion of reactants and products difficult during the catalytic process, which results in the decrease of activity.

Furthermore, the influence of reaction parameters, like temperature and gas pressure, was also investigated. On decreasing the reaction temperature to 60 °C, only 75.6% conversion and 68.5% aldehyde selectivity were obtained within the same reaction time (entry 6). In contrast, upon increasing the temperature to 80 °C, a conversion as high as 96.8% could be reached even within 3 h (entry 7). Notably, as the activity increases, a slightly higher aldehyde selectivity of 77.5% was obtained. On varying the CO/H$_2$ pressure, the reaction showed a similar tendency

that higher pressure induced better activity and aldehyde selectivity (Table 1, entries 8 and 9).

One of the most important advantages of organic–aqueous biphasic reaction systems is their recycling features. Here, the recyclability of the confined homogeneous catalysis system was firstly tested using Rh-TPPTS-0.97@HMSN as a model catalyst. After one cycle, the catalytic system was centrifuged, and the solid catalyst separated was used directly in another cycle after washing with toluene. As seen in Fig. S4 (ESI†), after centrifugation, the organic reaction phase was nearly colourless while yellow catalysts were deposited at the bottom. However, the catalytic activity drops dramatically. In the second cycle, only 35.0% conversion and 46.1% aldehyde selectivity could be obtained (entry 10). The loss of water solvent or rhodium active sites might account for this observation. To address this problem, we conducted a hydrophobic modification process with alkyl groups (including methyl and octyl groups).[31–33] Due to the existence of water, the modification process was easier to perform. As shown in Fig. S5 (ESI†), the surface properties of Rh-TPPTS-0.97@C$_1$-HMSN and Rh-TPPTS-0.97@C$_8$-HMSN become super-hydrophobic after modification, demonstrated by the large water contact angle (133° and 135° respectively). For the hydroformylation of 1-octene, the activity of these hydrophobic catalysts decreases a little. As shown in Table 1 (entries 11–14), the TOFs of Rh-TPPTS-0.97@C$_1$-HMSN and Rh-TPPTS-0.97@C$_8$-HMSN decrease from 623 to 378 and 558 h^{-1}, respectively. However, the recyclability of the confined solid catalyst in toluene could be improved after surface modification (Fig. S6, ESI†). For example, with Rh-TPPTS-0.97@C$_1$-HMSN as the catalyst, 95.4% conversion was still kept after four recycling tests. But for the aldehyde selectivity, it drops to 73.0% at the fourth cycle. As for Rh-TPPTS-0.97@C$_8$-HMSN, 81.2% conversion was maintained for the second cycle, which remained almost the same for the following two cycles. At the fourth cycle, 70.5% aldehyde selectivity was obtained. The selectivity variation might be related to the decreased catalytic activity, which induced a longer time to get the same conversion level. In addition, it is worth mentioning that compared with the product separation in the CTAB system or Pickering emulsion system, complicated separation processes could be avoided.

Encouraged by the above catalytic results, we then used other olefins, including 1-hexene, 1-heptene and 1-decylene, styrene, 4-methylstyrene and α-methyl styrene. As listed in Table 2, all the

Table 2 The hydroformylation of some olefins over Rh-TPPTS-0.97@HMSN^a

Entry	Substrate	Conv.^{b} (%)	Sel.^{b} (%)	n/b
1	1-Hexene	>99	79.5	71/29
2	1-Heptene	>99	78.0	69/31
3	1-Decylene^c	88.5	73.5	68/32
4	Styrene^d	>99	98	28/72
5	4-Methylstyrene^d	>99	99	29/71
6	α-Methyl styrene^d	>99	99	2/98

^{a} Reaction conditions: solid catalyst (Rh = 2.5 μmol), 7.5 mmol substrate, toluene as the solvent, 70 °C, 30 bar of CO/H$_2$, 4 h. ^{b} Analysis by GC. ^{c} Reaction time is 7 h. ^{d} 2.5 mmol substrate.

tested alkenes could be converted within a certain reaction time. The reaction rates and aldehyde selectivities for different substrates vary considerably. For example, with 1-hexene as a substrate, full conversion and 79.5% aldehyde selectivity could be obtained within only 4 h, while only 88.5% conversion and 73.5% aldehyde selectivity were obtained even within 7 h with 1-decylene as a substrate (entries 1–3). Notably, such a catalyst could also be expanded to the hydroformylation of aromatic alkenes, and almost full conversion was obtained with styrene, 4-methylstyrene or α-methyl styrene as substrates (entries 4–6).

In conclusion, hollow structured mesoporous silica nanospheres have been utilized as efficient nanoreactors for loading Rh-TPPTS aqueous solutions. Due to the small droplet sizes, the organic–aqueous interface area could be greatly enhanced, yielding improved catalytic activity and aldehyde selectivity in the biphasic hydroformylation of long-chain alkenes. Such a confined homogeneous catalysis system might be applied to other biphasic catalysis systems.

Conflicts of interest

There are no conflicts to declare.

Acknowledgements

Notes and references

1 R. Frank, D. Selent and A. Börner, *Chem. Rev.*, 2012, **112**, 5675–5732.
2 B. Breit, *Top. Curr. Chem.*, 2007, **279**, 139–172.
3 L. Obrecht, P. Kamer and W. Laan, *Catal. Sci. Technol.*, 2013, **3**, 541–551.
4 J. Potier, S. Menuel, M. H. Chambrier, L. Burylo, J. F. Blach, P. Woisel, E. Monflier and F. Hapiot, *ACS Catal.*, 2013, **3**, 1618–1621.
5 A. F. Cardozo, C. Julcour, L. Barthe, J. F. Blanco, S. Chen and F. Gayet, *J. Catal.*, 2015, **324**, 1–8.
6 K. Kunna, C. Müller, J. Loos and D. Vogt, *Angew. Chem., Int. Ed.*, 2006, **45**, 7289–7292.
7 J. P. Arhancet, M. E. Davis, J. S. Merola and B. E. Hnson, *Nature*, 1989, **339**, 454–455.
8 B. Tan, J. Y. Jiang, Y. H. Wang, L. Wei, D. J. Chen and Z. L. Jin, *Appl. Organomet. Chem.*, 2008, **22**, 620–623.
9 P. A. Zapata, J. Faria, M. P. Ruiz and D. E. Resasco, *Top. Catal.*, 2012, **55**, 38–52.
10 P. A. Zapata, J. Faria, M. P. Ruiz, R. E. Jentoft and D. E. Resasco, *J. Am. Chem. Soc.*, 2012, **134**, 8570–8578.
11 Z. W. Chen, L. Zhou, W. Bing, Z. J. Zhang, Z. H. Li, J. S. Ren and X. G. Qu, *J. Am. Chem. Soc.*, 2014, **136**, 7498–7504.
12 Z. W. Chen, C. Q. Zhao, E. G. Ju, H. W. Ji, J. S. Ren, B. P. Binks and X. G. Qu, *Adv. Mater.*, 2015, **28**, 1682–1688.
13 H. F. Liu, Z. M. Zhang and H. Q. Yang, *ChemSusChem*, 2014, **7**, 1888–1900.
14 M. Zhang, L. J. Wei, H. Chen, Z. P. Du, B. P. Binks and H. Q. Yang, *J. Am. Chem. Soc.*, 2016, **138**, 10173–10183.
15 M. P. Titus, L. Leclercq, J. M. Clacens, F. D. Campo and V. N. Rataj, *Angew. Chem., Int. Ed.*, 2015, **54**, 2006–2021.
16 Y. P. Zhao, X. M. Zhang, J. Sanjeevi and Q. H. Yang, *J. Catal.*, 2016, **334**, 52–59.
17 W. J. Zhang, L. M. Fu and H. Q. Yang, *ChemSusChem*, 2014, **7**, 391–396.
18 A. Riisager, R. Fehrmann, S. Flicker, R. van Hal, M. Haumann and P. Wasserscheid, *Angew. Chem., Int. Ed.*, 2005, **44**, 815–819.
19 M. Haumann, M. Jakuttis, S. Werner and P. Wasserscheid, *J. Catal.*, 2009, **263**, 321–327.
20 Y. S. Li and J. L. Shi, *Adv. Mater.*, 2014, **26**, 3176–3205.
21 X. M. Zhang, Y. T. Hou, R. Ettelaie, R. Q. Guan, M. Zhang, Y. B. Zhang and H. Q. Yang, *J. Am. Chem. Soc.*, 2019, **141**, 5220–5230.
22 T. J. Yoon, J. Kim and J. K. Lee, *Inorg. Chim. Acta*, 2003, **345**, 228–234.
23 Y. Yang, J. Liu, X. B. Li, X. Liu and Q. H. Yang, *Chem. Mater.*, 2011, **23**, 3676–3684.
24 L. Y. Jing, X. M. Zhang, R. Q. Guan and H. Q. Yang, *Catal. Sci. Technol.*, 2018, **8**, 2304–2311.
25 H. Chen, Y. Z. Li, J. R. Chen, P. M. Cheng, Y. E. He and X. J. Li, *J. Mol. Catal. A: Chem.*, 1999, **149**, 1–6.
26 B. Li, S. Y. Bai, X. F. Wang, M. M. Zhong, Q. H. Yang and C. Li, *Angew. Chem., Int. Ed.*, 2012, **51**, 11517–11521.
27 M. M. Zhong, X. M. Zhang, Y. P. Zhao, C. Li and Q. H. Yang, *Green Chem.*, 2015, **17**, 1702–1709.
28 Q. Sun, Z. F. Dai, X. L. Liu, N. Sheng, F. Deng, X. J. Meng and F. S. Xiao, *J. Am. Chem. Soc.*, 2015, **137**, 5204–5209.
29 H. N. T. Ha, D. T. Duc, T. V. Dao, M. T. Le, A. Riisager and R. Fehrmann, *Catal. Commun.*, 2012, **25**, 136–141.
30 X. Liu, S. Y. Bai, Y. Yang, B. Li, B. Xiao, C. Li and Q. H. Yang, *Chem. Commun.*, 2012, **48**, 3191–3193.
31 D. M. Santiburcio and D. Marx, *Chem. Sci.*, 2017, **8**, 3444–3452.
32 F. Hoffmann, M. Cornelius, J. Morell and M. Fröba, *Angew. Chem., Int. Ed.*, 2006, **45**, 3216–3251.
33 X. Rong, R. Ettelaie, S. Lishchuk, H. G. Chen, N. Zhao, F. K. Xiao, F. Q. Cheng and H. Q. Yang, *Nat. Commun.*, 2019, **10**, 1854.